Journal of Thermal Analysis, Vol. 54 (1998) 585-604

Application of TMDSC to polymeric systems

CHARACTERIZATION OF REACTING POLYMER SYSTEMS BY TEMPERATURE-MODULATED DIFFERENTIAL SCANNING CALORIMETRY

*S. Swier, G. Van Assche, A. Van Hemelrijck, H. Rahier, E. Verdonck and B. Van Mele**

Department of Physical Chemistry and Polymer Science, Vrije Universiteit Brussel
Pleinlaan 2, 1050 Brussels, Belgium

Abstract

The benefits of temperature-modulated differential scanning calorimetry to characterize reacting polymers are illustrated for different experimental systems. The effects of combined isothermal and non-isothermal cure paths on (de)vitrification, mobility-restricted reactions, and relaxation during vitrification are discussed for anhydride- and amine-cured epoxies. The simultaneous measurement of heat capacity, heat flow, and heat flow phase provides an excellent tool for mechanistic interpretations. The influence of the metakaolinite particle size on the production of inorganic silicate-metakaolinite polymer glasses is treated as an example. These principles are further illustrated for primary and secondary amine–epoxy step growth reactions, and for styrene-cured unsaturated polyester chain growth reactions with 'gel effect'. Finally, the effects of isothermal cure and temperature on reaction-induced phase separation in a polyethersulfone modified epoxy–amine system are highlighted.

Keywords: epoxy resin, inorganic polymer glass, reaction-induced phase separation, reaction mechanism, TMDSC, unsaturated polyester resin

Introduction

Differential scanning calorimetry (DSC) with a modulated temperature input signal (called TMDSC or MTDSC) has proven to be very beneficial for the thermal characterization of many materials, especially polymers. The simultaneous measurement of heat capacity, heat flow, and the phase angle between heat flow

* Author for correspondence: Tel: +32-(0)2-629.32.76; fax: +32-(0)2-629.32.78; e-mail: bvmele@vub.ac.be

1418–2874/98/ $ 5.00

Akadémiai Kiadó, Budapest
Kluwer Academic Publishers, Dordrecht

and heating rate (heat flow phase) also enables a more detailed study of reacting polymer systems, such as anhydride and amine curing epoxy resins, both in isothermal or quasi-isothermal [1, 2] and non-isothermal conditions [2, 3]. Vitrification and devitrification can be studied in relation to the applied reaction conditions. When appropriate experimental sampling, calibration, modulation and data handling procedures are followed, more reliable reaction kinetics can be deduced [4]. For the epoxy networks, the normalized heat capacity signal ('mobility factor') seems to describe the diffusion-controlled decrease in reaction rate ('diffusion factor') [1–3]. Using an empirical auto-catalytic conversion rate equation in combination with a modified WLF-equation, both isothermal and non-isothermal heat flow and heat capacity signals can be modelled [5]. As a result, the S-shaped vitrification curve in the Time–Temperature–Transformation and Continuous-Heating–Transformation diagrams [6, 7] can be quantified [8].

In contrast to these organic systems, the rate of the low-temperature production of inorganic silicate-metakaolinite polymer glasses (IPG) is nearly uninfluenced by the vitrification process [1].

While an empirical rate law for the global reaction conversion can be satisfactory, a mechanistic approach considering the evolution with time and/or temperature of different reacting species has several advantages. The influence of the initial composition of the reaction mixture, the rate constants of important reaction steps, and also morphological effects in heterogeneous reaction systems can be studied in a more systematic way.

A more detailed introduction of the phenomena describing the typical behaviour of reacting and thermosetting systems, including the glass transition temperatures T_{g0} and $T_{g\infty}$, the T_g-conversion relationship, gelation and vitrification, the shift from chemical to diffusion control of reactions, and complementary measuring techniques for the characterization of these properties is given in [1, 3, 5–7] and references cited therein.

In this paper, new TMDSC results will be presented to highlight the unique benefits of the technique to characterize reacting polymer systems. In some cases, additional information of dielectric analysis, dynamic mechanical analysis, and dynamic rheometry will be given. The effects of a combined cure path (partial isothermal cure followed by a non-isothermal postcure) will be discussed. The mechanistic information contained in the heat capacity, heat flow, and heat flow phase signals of TMDSC will be demonstrated. A phase separating ternary epoxy–amine/polyethersulfone will be introduced as an example of structure formation during cure.

Experimental

Epoxy systems

The following epoxy systems were studied: (1) stoichiometric mixtures of a tetrafunctional epoxy (Araldite MY 720) with a tetrafunctional amine hardener

(HY 2954); (2) stoichiometric mixtures of a bifunctional epoxy (DGEBA LY 556) with an anhydride hardener (HY 917) using 1 w% of an accelerator (1-methyl imidazole DY 070); all these components are from Ciba-Geigy, and are described in more detail in [1]; (3) monofunctional phenyl glycidyl ether PGE (Aldrich) cured with bifunctional aniline (Fluka) in molar ratios of amine/epoxy functional groups r=0.6 and r=1.0, respectively, and cured with bifunctional N,N'-dimethylethylenediamine A(sec) (Aldrich) for r=1.0; (4) bifunctional DGEBA LY 564 (Ciba-Geigy) cured with aniline for r=0.7 and r=1.0; (5) stoichiometric mixtures of DGEBA LY 564 with tetrafunctional methylenedianiline MDA (XU HY 205, Ciba-Geigy); (6) system (4) for r=1.0, combined with 20 w% of low molecular mass polyethersulfone PES (Aldrich). Epoxy systems (1)–(5) were mixed at room temperature until a clear mixture was obtained. To prepare system (6), PES was first dissolved in DGEBA at 120°C, then aniline was added at 90°C.

Inorganic polymer glasses

The inorganic polymer glasses (IPG) were produced by the reaction of an alkaline sodium silicate solution (Sil) with solid dehydroxylated clays (metakaolinite Mk). The molar ratio Sil/Mk was one. The materials and the sample preparation were described in [9]. To study the effect of particle size, Mk was fractionated by sedimentation of Mk suspensions in a water column of 25 cm height. Different fractions were collected with sedimentation times varying between 1 and 48 h. The particle size distribution of all Mk fractions was measured in water with a Coulter LS130, and was calculated using a Fraunhofer optical model. The following fractions were used, indicated as median of particle size d in μm (variance in μm^2): 13.0 (130), 3.1 (80), 1.8 (32), 1.5 (42).

Polyester–styrene systems

Two polyester systems were studied: (1) a mixture of unsaturated polyester resin with ca. 34 w% of styrene (Polylite P51383, Reichhold), methyl ethyl ketone peroxide initiator (Butanox M-60, Akzo Nobel), and 1% cobalt 2-ethylhexanoate in styrene accelerator (NL 49S, Akzo Nobel), in a w/w mixing ratio of 100/2/1; (2) a mixture of bisphenol-A based vinylester with ca. 48 w% of styrene (ATLAC 580, DSM), methyl ethyl ketone peroxide initiator (Butanox M-50, Akzo Nobel), and 6% cobalt 2-ethylhexanoate in dioctylphthalate accelerator (NL 51P, Akzo Nobel) in a w/w mixing ratio of 100/2/1.

Analytical techniques

The TMDSC experiments were performed on a TA Instruments 2920 DSC with MDSC™ option and equipped with two cooling systems: a refrigerated cooling system (RCS) and a liquid nitrogen cooling accessory (LNCA). Heat ca-

pacity was calibrated with polystyrene for the organic systems, and with water for IPG. All organic systems, with sample mass between 10 and 20 mg, were studied in aluminium pans with a 0.3–0.5°C per 60 s modulation. A 0.5°C per 100 s modulation was used for IPG, with sample mass of 50 mg, in reusable high-pressure stainless steel pans. More details on calibration, modulation conditions, and experimental procedure are given in [1–3].

The dielectric measurements were performed on a TA Instruments DEA 2970 equipped with a LNCA, using a ceramic single surface sensor in a frequency range from 1 Hz to 10^5 Hz. The dynamic mechanical analyses were performed on a Perkin Elmer DMA7 at 1 Hz. The special experimental set-up to follow the hardening process of IPG is described elsewhere [10]. The rheological measurements were performed on a TA Instruments AR 1000-N equipped with an extended temperature module (ETM), using a parallel plate geometry in the oscillation mode at 1 Hz.

Results and discussion

Mobility restrictions in isothermal, non-isothermal, and combined reaction conditions

The cure of epoxy–amine system (1) is studied with TMDSC and dielectric analysis in the same isothermal (Fig. 1) and non-isothermal reaction conditions (Fig. 2).

The mobility restrictions caused by vitrification during cure can be characterized either by a stepwise decrease in the heat capacity (quantified by $t_{1/2\Delta C_p}$ [1, 2] or $T_{1/2\Delta C_p}$ [2, 3]) or by an analogous stepwise decrease in the permittivity or by a local maximum in the dielectric loss factor [11–14]. While the frequency effect can easily be examined with DEA, indicating an increase of the glass transition temperature T_g of ca. 6°C per decade in frequency, this effect is very difficult to observe with TMDSC due to the limited range of applicable modulation periods. However, the major benefit of the latter technique is the simultaneous quantitative information on chemical conversion and conversion rate, enabling the cure kinetics to be established accurately [1–5, 8]. With TMDSC, mobility restricted cure kinetics and their effect on resulting material properties can be determined in terms of well-defined reaction paths.

Examples of non-isothermal post-cure experiments after a preceding partial cure with mobility restrictions are given for epoxy–anhydride system (2) in Fig. 3, and for epoxy–amine system (1) in Fig. 4. The combinations of partial cure time and temperature are chosen in a way that both systems (partially) vitrify before the final non-isothermal cure stage (see Fig. 1 for the amine system and [1, Fig. 7] for the anhydride system). For the epoxy–anhydride system, up to the isothermal onset of vitrification after 165 min of reaction at 85°C, no enthalpy relaxation is observed in the non-reversing heat flow signal of the subsequent heating (Fig. 3). As vitrification proceeds, due to the decreasing reaction

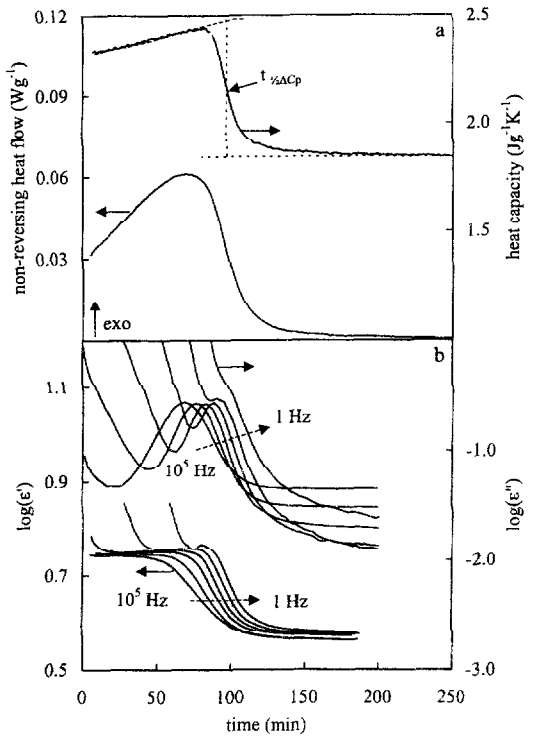

Fig. 1 Cure of epoxy–amine (1) at 70°C: (a) non-reversing heat flow and heat capacity; $t_{1/2\Delta C_p}$ ($-t_{v1t}$) is the time at half of the decrease in heat capacity; (b) permittivity, ε′, and dielectric loss factor, ε″, at 10^5, 10^4, 10^3, 10^2, 10 and 1 Hz

rate (controlled to a higher extent by diffusion) and the slow variation of T_g in these conditions, the structural relaxation effect is getting more pronounced [15, 16]. Figure 3 also shows the effect of the initial cure conditions on the residual reaction exotherm, getting more asymmetrical and delayed to higher temperatures. The increasing T_g of the system is acting as a physical barrier to the final cure. Nevertheless, at a heating rate of 2.5°C min^{-1}, this final cure always proceeds with a chemically-controlled rate. Note that T_g is still increasing considerably, even in mobility-restricted isothermal partial cure conditions, whereas the small residual reaction enthalpy is only slightly decreasing. $T_{g\infty}$ of this anhydride system is ca. 135°C (see heat capacity curve ⑥ of second heating after post-cure).

For the epoxy–amine system of Fig. 4, a different behaviour is observed. No relaxation effects are noticed in the non-reversing signal of the post-cure. In this case, even in diffusion-controlled isothermal conditions, the variation of T_g with reaction time is high enough to avoid this effect. Accordingly, at a heating rate of 2.5°C min^{-1}, only the initial part of the post-cure is chemically-controlled, as indicated by the heat capacity signals and the broad tails in the non-reversing heat

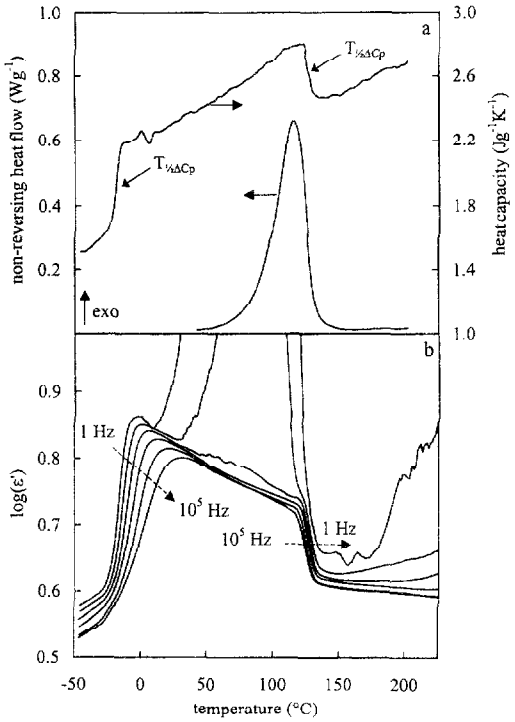

Fig. 2 Cure of epoxy–amine (1) at 3°C min^{-1}: (a) non-reversing heat flow and heat capacity; $T_{½\Delta C_p}$ ($=T_{vit}$ or T_{devit}) is the temperature at half of the step in heat capacity; (b) permittivity, ε', at 10^5, 10^4, 10^3, 10^2, 10 and 1 Hz

flow signals of Fig. 4. The start of mobility-restricted non-isothermal cure is interfering sooner with increasing conversion (reaction time) of the preceding isothermal cure. As soon as the heat capacity remains below the full mobility level (related to that conversion), the post-cure is (at least partially) diffusion-controlled over the entire range of the reaction exotherm (curves ④–⑦). $T_{g\infty}$ of this amine system is ca. 255°C and the upper devitrification is occurring at that temperature in all post-cure experiments (heat capacity curves ①–⑦).

Heat flow phase

Before briefly discussing some examples where TMDSC brings information about the mechanism of the reacting system, some remarks need to be made about the heat flow phase. The phase angle between modulated heat flow and modulated heating rate (called heat flow phase), corrected for instrument contributions of the TA Instruments 2920 MDSC™ [17], always remains small for the epoxy systems studied before [2, 4]. The same is valid for all reacting polymer systems discussed in this paper. Therefore, its influence on the quantitative na-

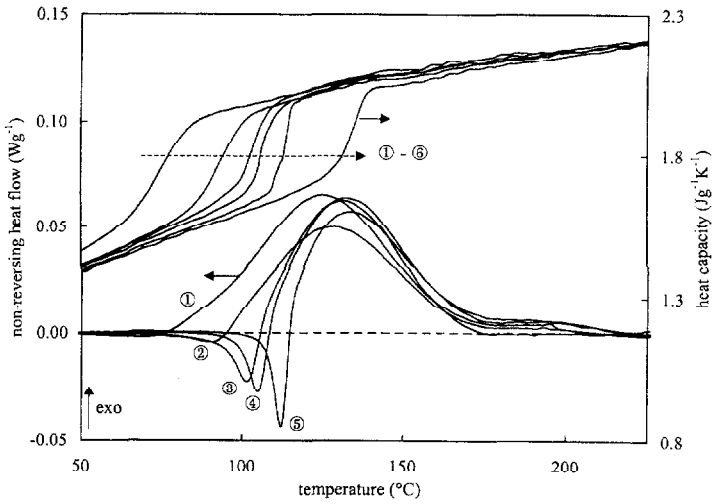

Fig. 3 Post-cure of epoxy–anhydride (2) at 2.5°C min^{-1}: non-reversing heat flow and heat capacity (1st heating) after partial cure at 85°C for 165 min (①), 230 min (②), 500 min (③), 800 min (④), 3300 min (⑤) and heat capacity (2nd heating) in same conditions (⑥)

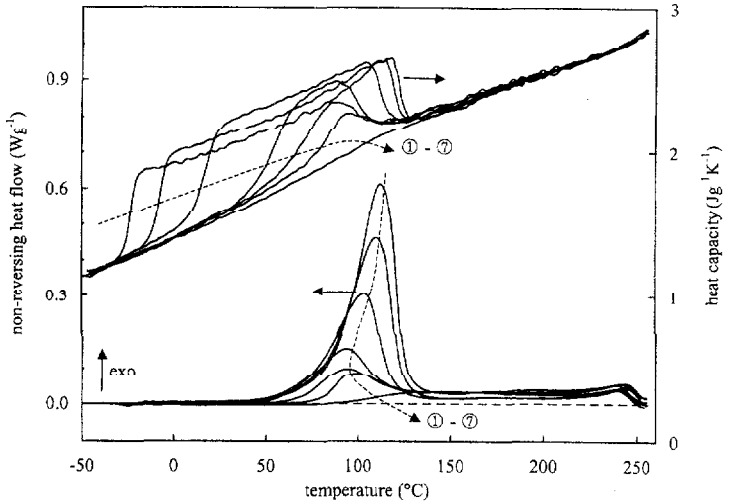

Fig. 4 Post-cure of epoxy–amine (1) at 2.5°C min^{-1}: non-reversing heat flow and heat capacity after partial cure at 70°C for 0 min (①), 25 min (②), 50 min (③), 75 min (④), 90 min (⑤), 110 min (⑥) and partial cure at 1.0°C min^{-1} to 116°C (=T_{vit}) (⑦)

ture of heat capacity and non-reversing heat flow is negligible too. However, the evolution of the phase angle over the course of the reaction contains valuable information on reaction and mechanism. The fully cured glass state is always used

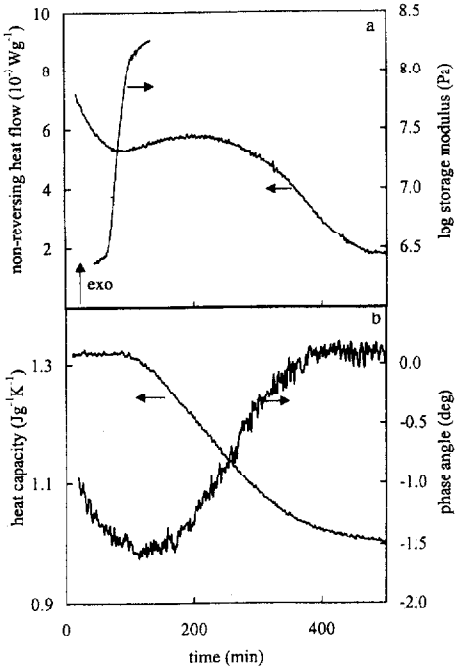

Fig. 5 Production of inorganic polymer glass for Mk particle size of 1.8 μm at 35°C; (a) non-reversing heat flow and storage modulus; (b) heat capacity and heat flow phase

as a reference (zero value) for the instrument correction [2, 4]. The phase angle corrected in this way has a small negative value, tending to more positive values due to the chemical reactions. Relaxation phenomena are superimposed as local (downward) extremes, indicating a vitrification or devitrification process during the thermal treatment. However, if the isothermal cure temperature is chosen close to the glass transition of the fully reacted polymer or network, $T_{g\infty}$, the system stays in the relaxation region at the end of cure, and the phase angle is not evolving to zero.

Inorganic polymer glasses: influence of particle size

The inorganic polymer glasses (IPG) are formed by the heterogeneous reaction of an alkaline sodium silicate solution (Sil) with dehydroxylated clays (metakaolinite Mk). The properties of the final amorphous aluminosilicates depend on the low-temperature reaction conditions [9, 10, 18]. The particle size of the solid reaction component, Mk, might also influence the reaction kinetics. To study this influence, the Mk was fractionated by sedimentation (see experimental). The heat flow, heat capacity and heat flow phase signals during production of IPG, measured at 35°C for different particle sizes, are shown in Figs 5 and 6.

For 1.8 μm particles, the concurrent hardening process is independently measured by dynamic mechanical analysis (Fig. 5). The onset of the steep increase in storage modulus (DMA) coincides with the onset of the heat capacity decrease (TMDSC), and a local minimum in the phase angle relaxation peak is observed at this early stage of the reaction. Whereas the DMA set-up is limiting the experimental window of moduli to follow the hardening process (both the low and high modulus values are not uniquely related to the IPG properties [10]), TMDSC enables to investigate the entire process via the heat capacity curve. This is important for studying these low-temperature IPG reactions, since vitrification is not slowing down the reaction rate and the largest part of the reaction enthalpy is set free in the solidifying state. A more detailed discussion is given in [1, 2, 10]. Figure 6 demonstrates the influence of the Mk particle size on the production rate of IPG. The heat flow signal is weak, especially for the largest grains, and therefore baseline instabilities are causing the signal to become less accurate. Anyhow, it is clear that the smaller the particle size, the larger the heat flow at the beginning of the reaction and the faster the reaction tends to completeness. However, in the conditions studied, the heat capacity signal is still accurate

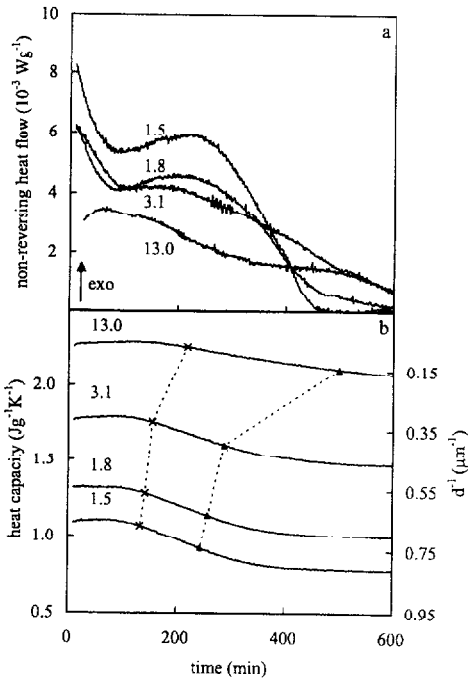

Fig. 6 Production of inorganic polymer glasses for different Mk particle sizes (indicated values in μm) at 35°C: (a) non-reversing heat flow; (b) heat capacity (shifted downward according to initial reciprocal particle diameter, d^{-1} (right Y-axis); only for the largest particles (upper curve), the heat capacity scale is valid) with t(10%) (×) and t(50%) (▲); dotted lines are only a guide to the eye

and free of baseline instabilities, and again allows the reaction to be followed long after the onset of vitrification. Even for the smallest particles, the heat capacity is still decreasing after 3000 min of reaction (not shown in Fig. 6). The effect of particle size on the reaction rate can now be quantified based on the reaction time to reach a certain decrease in heat capacity, for example times for a drop of 10 or 50% in heat capacity. In Fig. 6b, the times $t(10\%)$ and $t(50\%)$ are indicated on the heat capacity curves. The trends depicted by the interconnecting dotted lines show the effect of the initial reciprocal diameter, d^{-1} (plotted on the right Y-axis), which is proportional to the initial specific surface of the particles. It can be deduced that the reaction rate increases with decreasing particle size or increasing specific surface. For the largest specific surfaces, however, this tendency seems to level off. These conclusions are important for a more elaborated model of the heterogeneous reaction kinetics of IPG [19].

Free-radical chain growth polymerization: gel effect

Although the autoacceleration or 'gel effect' in free radical polymerization is well understood in general terms of a decrease in the mobility of growing chains, quantitative results on detailed aspects to develop more predictive models, including for example a varying initiator efficiency and chain length dependent ter-

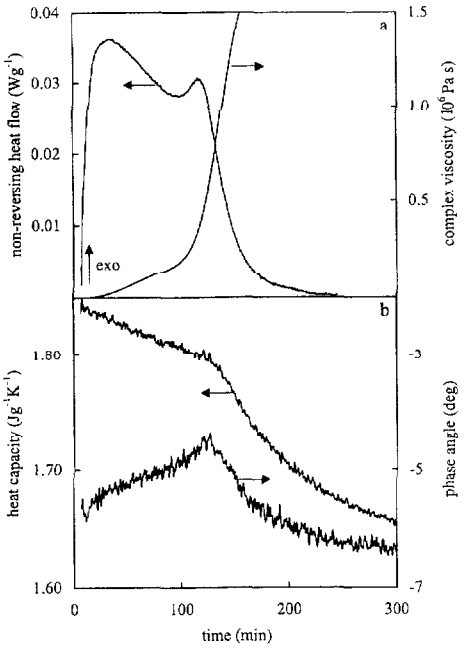

Fig. 7 Cure of polyester–styrene (1) at 30°C: (a) non reversing heat flow and complex viscosity; (b) heat capacity and heat flow phase

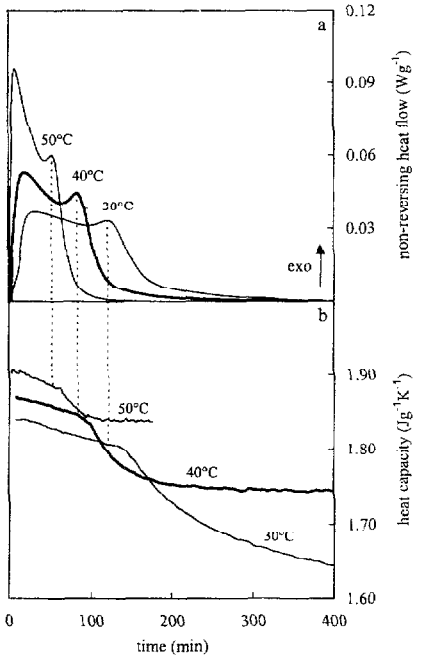

Fig. 8 Cure of polyester–styrene (1) at 30, 40 and 50°C: (a) non-reversing heat flow; (b) heat capacity

mination, are still scarce [20]. One of the major reasons is the difficulty of maintaining isothermal conditions in bulky samples, and the lack of truly isothermal conversion-time data and reliable rate constants. Isothermal conventional DSC is suggested to be advantageous in collecting these data [20]. The additional benefits of temperature modulated DSC are illustrated for two polyester–styrene systems, reacting by free-radical copolymerization [21]. The non-reversing heat flow at 30°C of polyester–styrene system (1) is compared with rheological information in Fig. 7a. The typical autoacceleration observed in the heat flow signal coincides with the ultimate increase of the complex viscosity (beyond a certain level), but occurs just before the onset of vitrification as shown by the heat capacity and heat flow phase signal in Fig. 7b. The heat flow phase signal also indicates that the system is remaining in the relaxation regime, even at the end of cure at 30°C, due to a low value of $T_{g\infty}$ of ca. 25–28°C.

These observations can be generalised to other isothermal conditions in Fig. 8. With increasing temperature, the aspect of the reaction exotherm is changing by a relatively less important 'gel effect' (Fig. 8a); the extent of (partial) vitrification reached afterward is decreasing, but still visible at 50°C (Fig. 8b). Typical for these polyester systems is a broad glass transition domain of at least 50°C around $T_{g\infty}$. Due to the effect of this broad transition domain, par-

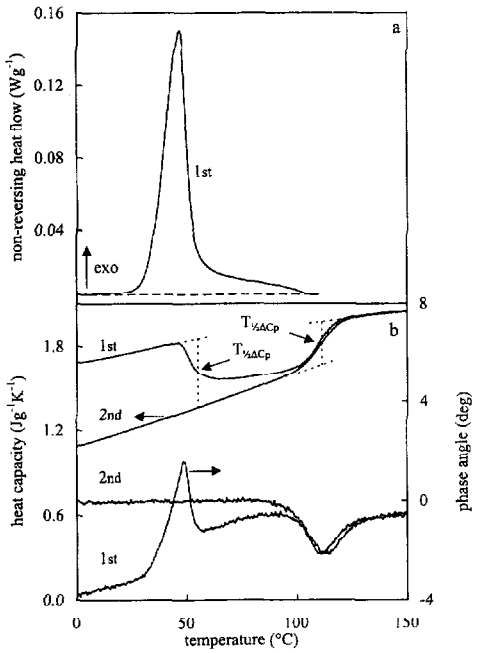

Fig. 9 Cure of vinylester–styrene (2) at 0.5°C min^{-1}: (a) non-reversing heat flow for 1st heating; (b) heat capacity and heat flow phase for 1st and 2nd heating; $T_{1/2\Delta C_p}$ (=T_{vit} or T_{devit}) is the temperature at half of the step in heat capacity

tial vitrification occurs in all isothermal conditions shown, even at 50°C. A model including initiation, propagation, transfer, inhibition, and termination steps should be used to describe the 'gel effect' in combination with the role of parameters such as temperature and concentration of inhibitor and reactive solvent from zero up to high reaction conversion. Such a mechanistic model should deal with termination and propagation rates controlled in a different way by mobility or diffusion, using the simultaneous TMDSC information of heat flow and heat capacity (with heat flow phase), respectively [22].

Figure 9 shows the non-isothermal cure of vinylester–styrene system (2) heated at 0.5°C min^{-1}. A diffusion-controlled regime, observed as a broad shoulder beyond the reaction exotherm in the non-reversing heat flow and as a decrease in the heat capacity, is extending over more than 60°C. Note that this is not caused by a very high value of $T_{g\infty}$ (see also [3]), which is only ca. 110°C in this case, but by the high reactivity of the system. This high reactivity is also noticed in the heat flow phase, with a peak going through slightly positive values in the first heating (Fig. 9b). The position of $T_{g\infty}$, observed by the devitrification after the diffusion-controlled reaction in the first heating (stepwise increase in heat capacity and relaxation peak in the heat flow phase), is confirmed in the second heating.

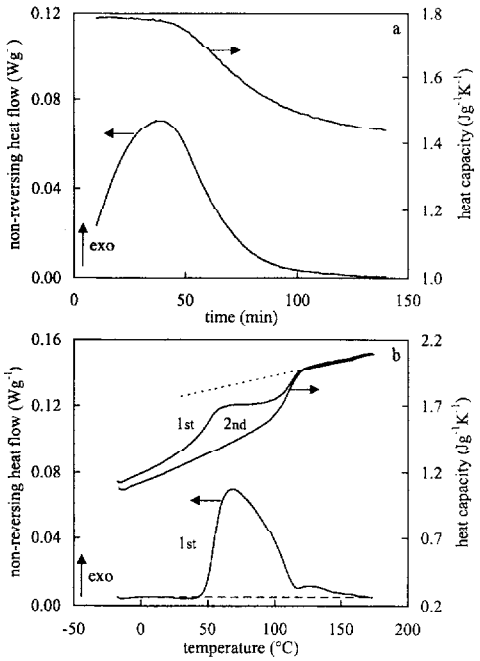

Fig. 10 Non-reversing heat flow and heat capacity of vinylester–styrene (2): (a) cure at 40°C for 140 min; (b) post-cure at 2.5°C min^{-1}: 1st and 2nd heating

Figure 10a shows a partial cure at 40°C for 140 min of the same vinylester–styrene system (2), followed by a non-isothermal post-cure at 2.5°C min^{-1} (Fig. 10b). After vitrification at 40°C, the system does not enter a fully chemically-controlled post-cure, even when heated at 2.5°C min^{-1}. When the material starts devitrifying in the first heating, the residual reaction immediately starts, causing a partial revitrification. Therefore, the remaining reaction exothermicity is set free in partially diffusion-controlled conditions. Finally, the small tail at higher temperatures (only 2% of the total reaction enthalpy) might again be a fully chemically-controlled post-cure regime. The position of $T_{g\infty}$ is observed in the heat capacity curve of the second heating (Fig. 10b). Note that a 'gel effect' is not obvious in the experiments of Figs 9 and 10, but probably should also be taken into account when modelling these reactions.

Step growth polymerization: primary and secondary amine reactions

The importance for mechanistic investigations of the measurement of the heat capacity change in (quasi)isothermal reaction conditions is further demonstrated in Figs 11 and 12 for the addition reactions or step growth polymerizations of epoxy–amine systems (3), (4), and (5). An important difference between PGE–aniline (3), DGEBA–aniline (4), and DGEBA–MDA (5) is the functionality of the

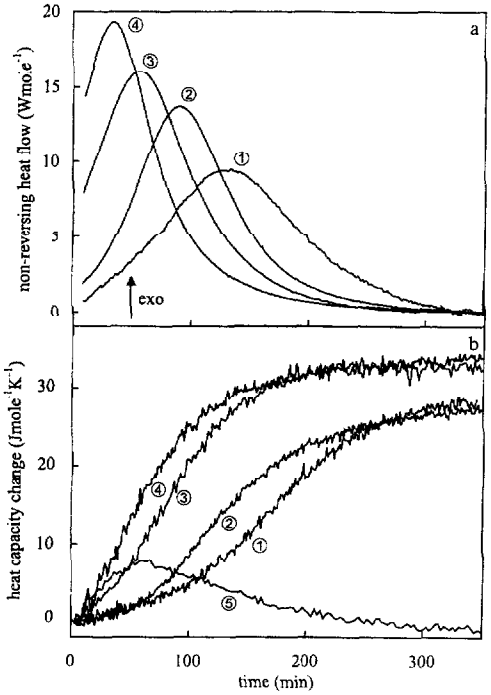

Fig. 11 Cure at 100°C of epoxy–amine (3) for r=0.6 (①), r=1.0 (②) and of epoxy–amine (4) for r=0.7 (③) and r=1.0 (④): (a) non-reversing heat flow per mole of reacted (epoxy–NH) functional groups; (b) heat capacity change per mole of reacted (epoxy–NH) functional groups; PGE–A (sec) at 30°C is given for comparison (⑤)

reactive components, leading in stoichiometric conditions to small molecules ($T_{g\infty}$=–4°C), linear macromolecules ($T_{g\infty}$=75°C), and a polymer network ($T_{g\infty}$=102°C), respectively. The differences in the rate of cure, caused by the nature of the epoxy or the mixing ratio r (Fig. 11), or by the nature of the amine in combination with the isothermal temperature (Fig. 12), are visible.

It is obvious that the heat capacity first increases to a maximum value (plateau), followed in some cases by an important decrease. This evolution is already observed in Fig. 1 for epoxy–amine system (1), and is in agreement with the observation in Fig. 4 that ΔC_p at T_g first increases with increasing isothermal conversion. Analogous observations were made for an isothermal epoxy–amine reaction using a specially designed microcalorimetric technique [14, 23, 24]. It should be noted that in all experimental conditions of Figs 11 and 12, primary amine–epoxy in combination with secondary amine–epoxy addition reactions are predominant in the reaction mechanism [25–27]. For comparison, the heat capacity curve for PGE–A(sec) is also depicted in Fig. 11b, showing the striking difference when only secondary amine functionalities can react. Note that this aliphatic secondary amine system was measured at 30°C, to reach full conversion

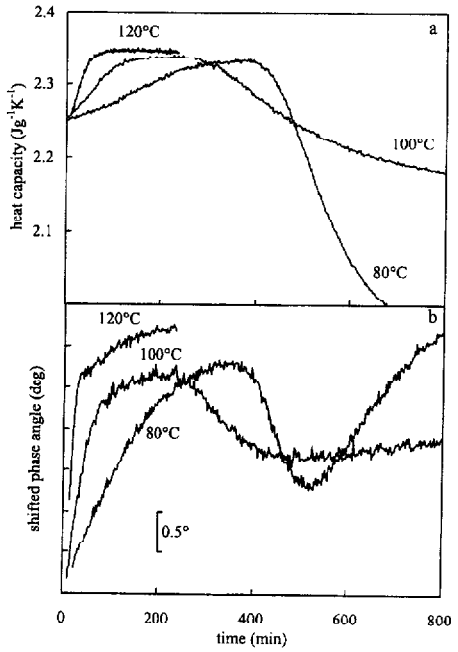

Fig. 12 Cure of epoxy–amine (5) at 80, 100 and 120°C: (a) heat capacity; (b) heat flow phase (shifted for clarity)

in a comparable time scale as the less reactive aniline systems at 100°C. The ability of TMDSC to make distinction between primary and secondary amine–epoxy reactions can be explained in terms of a group additivity estimation method of thermodynamic properties of organic compounds at 298.15 K in the liquid and solid phase [28]. According to this method, primary amine–epoxy reactions always give rise to positive variations in heat capacity, whereas the predicted changes in heat capacity for secondary amine–epoxy reactions are almost zero or even negative (depending on the aliphatic or aromatic nature of the secondary amine). The experimental values of $\Delta C_{p,react}$ (at full conversion of the functional group present in minority) for PGE–aniline (3) and DGEBA–aniline (4) at 100°C are in agreement with these predictions. Indeed, the heat capacity curves of Fig. 11b reach a comparable limiting value, both for stoichiometric mixtures and for mixtures with an excess of epoxy ($r \leq 1.0$). The heat capacity curve for PGE–A(sec) is also in agreement with the predicted variation for secondary amine–epoxy reactions. Note that in the case of an excess of amine ($r > 1.0$; not shown in Fig. 11), the ratio of the reactivity of secondary and primary amines (substitution effect) is influencing the value of $\Delta C_{p,react}$ at full conversion of epoxy.

The measurements of $\Delta C_{p,react}$ at full conversion can be disturbed by vitrification, as illustrated with the heat capacity and the heat flow phase signals of DGEBA–MDA in Fig. 12. At 80°C, a relaxation peak is observed, while at

100°C, the system is partially vitrifying and the phase angle remains in the relaxation regime at the end of cure. In comparison with conventional DSC [29], the examples of Figs 11 and 12 illustrate the additional benefits of TMDSC to investigate mechanism, kinetics, and rate constants of reaction steps of epoxy–amine cure.

Reaction-induced phase separation

Precursors of specially designed architecture seem to play an important role in future developments of polymer network structures with improved properties [30]. The formation of a liquid crystalline order in (epoxy) thermosets is one example [31]. Reaction-induced phase separation in modified thermosetting polymers is another aspect [32, 33]. As a final example of the power of TMDSC to get insight in these complicated reacting polymer systems, a stoichiometric mixture of DGEBA–aniline together with 20 w% of PES is studied. The reaction-induced phase separation in isothermal conditions, due to growing linear macromolecules with increasing molecular mass, and the effect of a thermal post-treatment are shown in Figs 13 and 14. The heat capacity for the PES-modified system starts decreasing after a certain reaction time (Fig. 13b), instead of increasing to a plateau, as observed (curves ①) and expected for an isothermal cure of

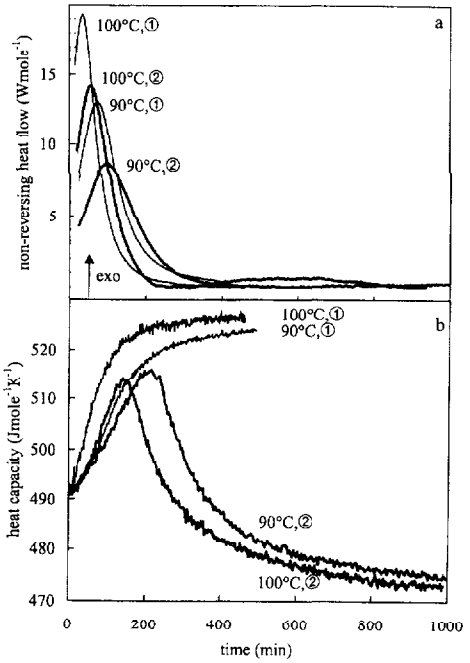

Fig. 13 Cure at 90 and 100°C of epoxy–amine (4) for r=1.0 (①) and of epoxy–amine (6) showing reaction-induced phase separation (②); (a) non-reversing heat flow per mole epoxy equivalent; (b) heat capacity per mole epoxy equivalent

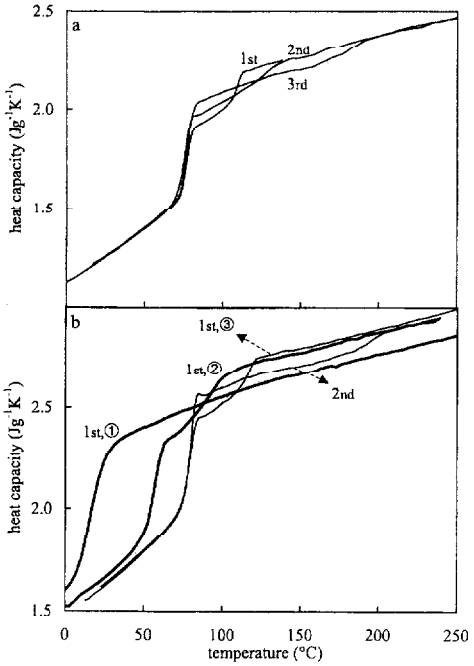

Fig. 14 Reaction-induced phase separation of epoxy–amine (6): (a) influence of thermal post-treatment at 5°C min^{-1}, after cure at 90°C for 1300 min (Fig. 13): heat capacity of 1st heating to 150°C, 2nd and 3rd heating to 280°C; (b) influence of cure time, t, at 100°C (Fig. 13): heat capacity of subsequent 1st heating at 5°C min^{-1} for t=80 min (①), t=180 min (②), t=1000 min (③) and 2nd heating at 5°C min^{-1} (valid for ①, ② and ③)

pure DGEBA–aniline at 90 or 100°C ($T_{g\infty}$=75°C). This effect is not caused by vitrification of the epoxy–amine matrix, but by vitrification of a PES-rich dispersed phase, separating out at this stage of the isothermal reaction. Modelling of the cure kinetics is necessary to decide whether the changed cure rate of the initially homogeneous mixture, as seen in the non-reversing heat flow (Fig. 13a), and indirectly also in the heat capacity (Fig. 13b), is caused by the dilution effect of PES, by changing rate constants or new reaction steps in the autocatalytic mechanism. After full cure at 90°C, the additional influence of temperature on the reaction-induced phase-separated system is demonstrated in Fig. 14a. The heat capacity curves of the first, second and third heating show the phases formed at 90, 150 and 280°C, respectively. The mass fraction of the epoxy-rich phase is increasing, but T_g remains almost constant at 75–77°C, in contrast with the PES-rich phase with a strongly increasing T_g from ca. 110 to ca. 180°C (with an upper onset value of 190°C, in comparison with a T_g of of ca. 225°C for pure PES). This evolution of mass fractions and compositions of the phases with increasing temperature supports a phase separating behaviour with an asymmetrical 2-phase

domain and a 'lower critical solution temperature' (LCST) in the phase diagram [33].

The heat capacity curves of Fig. 14b show the influence of the cure time, t, at 100°C. For t=80 min, before the maximum in the heat capacity evolution (see Fig. 13b, 100°C curve ②), the partially cured PES-modified DGEBA–aniline is still homogeneous with T_g=15°C (in comparison with T_{go}=–40°C for the uncured system). After the maximum of the heat capacity in Fig. 13b, the system becomes heterogeneous. With increasing cure time, t, the difference in T_g between the phases is getting larger suggesting a broadening of the 2-phase domain in combination with a lowering LCST as a function of increasing molecular mass of the curing matrix [33]. Note that without a preceding partial or full cure, for example in the same system without aniline (DGEBA + 20 w% PES), no phase separation is observed when heating twice to 280°C and T_g remains at the initial value of ca. –16°C. In this case, the value of LCST seems to be beyond 280°C.

Conclusions and future developments

TMDSC is a powerful thermal analysis technique to characterize important events along the reaction path of reacting polymer systems. An empirical modelling of both heat flow and heat capacity TMDSC signals in isothermal and/or non-isothermal reaction conditions enables the quantification of the influence of vitrification and devitrification on the reaction kinetics. In this way, the cure kinetics can be determined more accurately than with conventional DSC, even up to high overall reaction conversion [4, 5, 8].

The combined information of heat capacity, heat flow, and heat flow phase also provides an excellent tool for more detailed mechanistic studies of reacting polymer systems. The change in heat capacity due to chemical reactions, measured as a function of the conversion and/or the composition of the initial reaction mixture, gives valuable constraints in determining the rate constants of important reactive species involved in the mechanism. The effects of the type of reaction mechanism, e.g. step growth *vs.* radical chain growth, addition *vs.* condensation, or organic *vs.* inorganic, can be investigated in a systematic way.

TMDSC is also excellent for studying reacting systems with structure formation along the reaction path. Reaction-induced phase separation of a thermoplastic additive is one example, the formation of liquid crystalline thermosets is another one. In these cases, the influence of the dispersed phase on the reaction kinetics of the matrix can be investigated with an improved sensitivity. This is of extreme importance for the production of modified thermosetting polymers and also thermoset composites, especially when the additive (or reinforcing fiber) itself is able to react with the matrix components, and interphase regions are developing. A very interesting extension is the study of interpenetrating networks. In this case, not only the final properties of the network structure can be evaluated

using heat capacity and derivative signals [34], but also the influence of the in situ production. All research topics mentioned in this paper are in progress and will be explored further in the near future.

* * *

The work of S. Swier, G. Van Assche, A. Van Hemelrijck and E. Verdonck was supported by grants from the Flemish Institute for the Promotion of Scientific-Technological Research in Industry (I.W.T.).

References

1 G. Van Assche, A. Van Hemelrijck, H. Rahier and B. Van Mele, Thermochim. Acta, 268 (1995) 121.
2 G. Van Assche, A. Van Hemelrijck, H. Rahier and B. Van Mele, Thermochim. Acta, 304–305 (1997) 317.
3 G. Van Assche, A. Van Hemelrijck, H. Rahier and B. Van Mele, Thermochim. Acta, 286 (1996) 209.
4 G. Van Assche, A. Van Hemelrijck and B. Van Mele, J. Thermal Anal., 49 (1997) 445.
5 A. Van Hemelrijck, Ph.D. Thesis, Department of Physical Chemistry and Polymer Science, Free University of Brussels, 1996; A. Van Hemelrijck and B. Van Mele, to be published.
6 G. Wisanrakkit and J. K. Gillham, J. Coat. Technol., 62 (1990) 35.
7 J. K. Gillham and J. B. Enns, Trends in Polymer Sci., 2 (1994) 406.
8 A. Van Hemelrijck and B. Van Mele, J. Thermal Anal., 49 (1997) 437.
9 H. Rahier, B. Van Mele, M. Biesemans, J. Wastiels and X. Wu, J. Mater. Sci., 31 (1996) 71.
10 H. Rahier, B. Van Mele and J. Wastiels, J. Mater. Sci., 31 (1996) 80.
11 S. D. Senturia and N. F. Sheppard, Jr., Adv. Polym. Sci., 80 (1986) 1.
12 K. A. Nass and J. C. Seferis, Polym. Eng. Sci., 29 (1989) 315.
13 M. G. Parthun and G. P. Johari, Macromolecules, 25 (1992) 3149.
14 M. Cassettari, G. Salvetti, E. Tombari, S. Veronesi and G. P. Johari, J. Non-Cryst. Solids, 172–174 (1994) 554.
15 S. Montserrat, J. Appl. Polym. Sci., 44 (1992) 545.
16 J. M. Hutchinson, D. McCarthy, S. Montserrat and P. Cortes, J. Polym. Sci. Part B: Polym. Phys., 34 (1996) 229.
17 M. Reading, D. Elliott and V. L. Hill, Proc. NATAS Conference 1992, p. 145.
18 H. Rahier, W. Simons, B. Van Mele and M. Biesemans, J. Mater. Sci., 32 (1997) 2237.
19 H. Rahier and B. Van Mele, J. Mater. Sci., to be published.
20 G. A. O'Neil and J. M. Torkelson, Trends in Polymer Sci., 5 (1997) 349.
21 G. L. Batch and C. W. Macosko, J. Appl. Polym. Sci., 44 (1992) 1711.
22 G. Van Assche, E. Verdonck and B. Van Mele, to be published.
23 M. Cassettari, G. Salvetti, E. Tombari, S. Veronesi and G. P. Johari, J. Polym. Sci. Part B: Polym. Phys., 31 (1993) 199.
24 M. Cassettari, F. Papucci, G. Salvetti, E. Tombari, S. Veronesi and G. P. Johari, Rev. Sci. Instrum., 64 (1993) 1076.
25 J. Mijovic, A. Fishbain and J. Wijaya, Macromolecules, 25 (1992) 979.
26 B. Fitz, S. Andjelic and J. Mijovic, Macromolecules, 30 (1997) 5227.
27 S. Andjelic, B. Fitz and J. Mijovic, Macromolecules, 30 (1997) 5239.
28 E. S. Domalski and E. D. Hearing, J. Phys. Chem. Ref. Data, 22 (1993) 805.
29 S. Vyazovkin and N. Sbirrazzuoli, Macromolecules, 29 (1996) 1867.

30 K. Dusek, Trends in Polymer Sci., 5 (1997) 268.
31 J. S. Grebowicz, Macromol. Symp., 104 (1996) 191.
32 I. Alig, W. Jenninger, M. Junker and L. A. de Graaf, J. Macromol. Sci.-Phys., B35 (1996) 563.
33 R. J. J. Williams, B. A. Rozenberg and J. P. Pascault, Adv. Polym. Sci., 128 (1997) 95.
34 M. Song, D. J. Hourston, H. M. Pollock, F. U. Schäfer and A. Hammiche, Thermochim. Acta, 304–305 (1997) 335.